Simulated and Measured Surface Roughness in High Speed Grinding of Silicon Carbide Wafers

CHEN Shan Shan[1,2*], Cheung Chi Fai [2], ZHAO, Chen Yang [2], ZHANG Fei Hu[1]

1 Harbin Institute of Technology, School of mechanical and electrical engineering, Harbin, China
2 Partner State Key Laboratory of Ultraprecision Machining Technology, Department of Industrial and Systems Engineering, The Hong Kong Polytechnic University, Hung Hom, Kowloon, Hong Kong,
*Corresponding author: chenshanshan2009@163.com Fax: (852)23625267

Abstract: In this paper, the primary factors affecting the surface quality are studied and a theoretical model is developed for surface generation in grinding Silicon Carbide (SiC). The model takes into account the geometrical kinematics and tool micro-vibration in grinding operation. The simulated roughness profile agree reasonably well with experimental results. Spectrum analysis extracts three different frequencies from the machined surface topography in frequency domain, figure error, micro-vibration of the wheel and workpiece respectively. The wheel synchronous micro-vibration is found to be the dominant mechanism for surface generation. The pattern of vibration marks is found to depend on the feed rate and the ratio of the rotational speed of grinding wheel and the workpiece. In addition, the phase shift denoted the fractional part of the speed ratio is inevitably induced in the evolution of surface generation in grinding, which imposes a remarkable effect on surface quality, for non-integral speed ratio, arithmetical mean height of the surface (Sa) is significantly improved about 0.108μm. Medium phase shift (about 0.5) can suppress scallop-height so as to improve surface quality. The results provide an important mean for improving the surface quality in ultra-precision grinding.

Key words: Silicon carbide; Grinding; Surface generation; Modelling; Simulation; Micro-vibration

1 Introduction

In recent years, space optical technology has escalated the demand for manufacturing of large aspheric lenses and mirrors. Silicon carbide (SiC) as an advanced engineering ceramic is becoming a preferred material for precision optical components due to its excellent performance in thermal shock, wear resistance, high stiffness, structural stability and chemical inertness [1-4]. However, SiC is a difficult-to-machine material due to extremely high hardness and low fracture toughness [5,6]. In order to produce a super mirror finished surface, great effort has focused on using different ultra-precision machining technologies for machining SiC. They include single-point diamond turning [7], lapping [8], ultra-precision grinding [9] and computer controlled polishing [10]. Among these ultra-precision machining technologies, ultra-precision grinding is one of the most widely used process for machining SiC ceramic due to high efficiency and less damage.

However, ultra-precision grinding is a complex process involving various effects and stochastic natures caused by the behavior of irregular abrasive grits in the cutting zone, which imposes a formidable challenge to study the mechanism of surface generation and dynamics analysis of the grinding process [11-13].

For machining super hard ceramic materials, higher cutting forces are produced for machine tools, which triggers the

larger grinder deformation and motion errors than machining traditional plastic materials. To fabricate a super mirror finished surface with high dimensional tolerance and form accuracy, extensive research has been performed to study surface generation in ultra-precision grinding of ceramic materials. There are two mechanisms for the surface generation in machining ceramics which include brittle fracture and ductile material removal [14-17]. Ceramic components are prone to have a smooth surface in ductile mode [18-20].

Bifano [21] developed a model based on the maximum chip thickness to predict the fracture damage. The model established the critical depth of cut for ductile material removal.Yin [22] et al investigated the effects of machining conditions on surface finish in grinding polycrystal SiC. Fawcett and Storz [22] have established a geometric model according to the kinematic of the interaction of the workpiece and the grinding wheel so as to simulate the surface generation. Cheng and Gong [23] investigated micro-interacting mechanisms (i,e. ductile, brittle-ductile and brittle) in the surface generation of grinding single crystal silicon. Chip geometry play an important role in the surface formation in machining, which provides a lot of physical information in cutting zone[25-26]. Zhang [24] et al constructed a model to calculate the maximum undeformed chip thickness in face grinding. Jiang, Ge and Hong [24] established a microscopic model to represent micro-interacting mechanism of cutting edges in grinding contact area considering different sizes, locations and protruding heights of the abrasive grains to predict surface roughness. Zhang [26] et al investigated changes of surface layer in machining silicon wafers using single diamond scratching. Yin et al study the influence of grit size on surface generation in grinding 6H-SiC(0001) substrates. Chen, Fang and Li [25] study the influence of the vibration of the grinding wheel on the surface evolution and they established a model of surface profile generation.

At present, most of research considered the study of grit geometry, operation parameters and the interaction of abrasive grains and workpiece or the vibration of grinding wheel so as to uncover the mechanism of surface generation. However, they overlooked the synthesis of phase shift and micro-vibration. The vibration problem with phase shift has received relatively little attention. In fact, it can change the relative position of the wheel to the workpiece and this exerts a significant impact on surface quality and surface topography. This paper attempts to develop a surface generation model by considering the phase shift and micro-vibration and power spectral analysis is used to verify the simulation results.

2. Modeling of Surface Generation in Ultra-precision Grinding

In this study, the surface generation in ultra-precision grinding is modeled based on the machine configuration as shown in Fig .1. In ultra-precision grinding, both the grinding wheel and the workpiece rotate anticlockwise (up-grinding). The ground surface generated by the high-speed spinning wheel traverses a rotating workpiece (V_1) at a fine feed rate (V_f). Under ideal condition, the surface topography is transferred by the envelope of fixed abrasives on the grinding wheel as shown in Fig. 2. Grinding parameters can be used to determine the trajectory of the grinding wheel with respect to the workpiece, which results in different patterns of surface topographies. As shown in Fig. 3, the periodical structure of the

machined surface consists of the peripheral feed distance (pf) per one revolution of grinding wheel traveled the workpiece and the cross feed distance (S) of the tool traversed for each revolution of the workpiece. Both of them can be determined by Eq. (1) and Eq. (2), respectively. r is the distance between cutting point and the machining center.

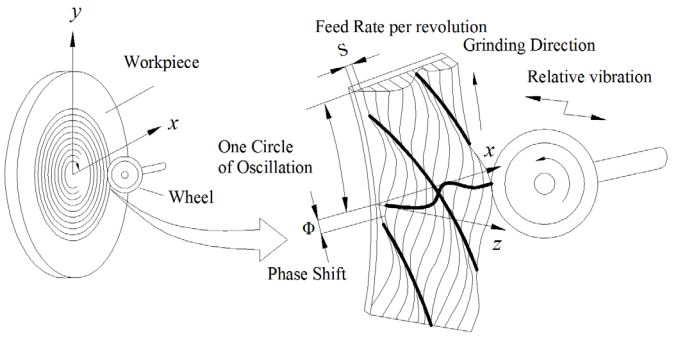

Fig.1 Cutting mechanics of ultra-precision grinding under micro-vibration

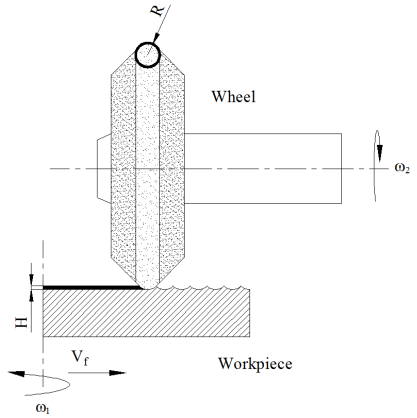

Fig. 2 Ideal surface produced by an arc-shaped grinding wheel

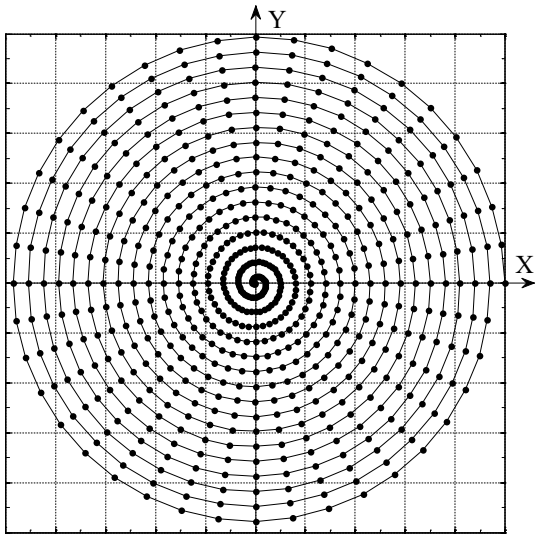

Fig. 3 Periodical structure of machined surface

$$pf = \frac{2\pi V_2 r}{V_1} \tag{1}$$

$$S = \frac{V_f}{V_2} \tag{2}$$

In order to avoid the disturbance of original surface profile, the SiC workpiece is ground by fine grinding firstly. At the same time, accurate dynamic balance work is conducted for both the workpiece spindle and the grinding wheel spindle before actual experiments.

2.1 Modeling of Spiral Marks Generation

In ultra-precision grinding of SiC, the grinding tool is difficult to cut into the material with extremely high hardness. The force generated in the grinding process causes the deflection of the tool and grinder, which affects the accuracy and surface finish of the workpiece. Especially, the normal deflection of the grinding wheel causes the rotational center does not match the concentric center of the rotation axis, which induces the spindle unbalance as shown in Fig. 4.

This kind of periodic deflection degraded the surface quality and caused surface waviness. In reality, it is impossible to entirely eliminate the unbalance in the grinding although excellent static and dynamic balance work have been carried out both for workpiece spindle and the grinding wheel. Such vibration ultimately effects surface generation of the workpiece and results in the generation of the spiral marks on the ground surface. The primary vibration frequency is synchronous with the rotational speed of the grinding wheel. The number of spiral marks (N) is equal to the integer of the ratio of the rotational speed of the grinding wheel (V_1) and the rotational speed of the workpiece (V_2). The fraction of the ratio attributes to the accumulation of phase shift, which alleviates average waviness of the ground surface.

$$N = \frac{V_2}{V_1} \tag{3}$$

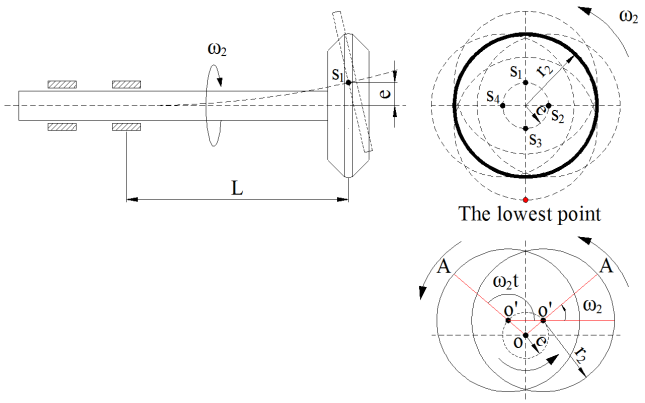

Fig. 4 Synchronous micro-vibration caused by the deflection of the shank of the grinding wheel

Fig. 1 shows the generation mechanism of the spiral marks. If the rotational speed of the wheel is equal to integer multiple of the part rotational speed, there is no phase shift and the surface waves keep stable in every revolution as shown in Fig. 5(a). However, if the ratio is a non-integral number, a phase shift of the wave on the ground surface occurs in each

subsequent revolution of the workpiece. It can suppress amplitude of surface waves and improve the surface quality as shown in Fig. 5(b).

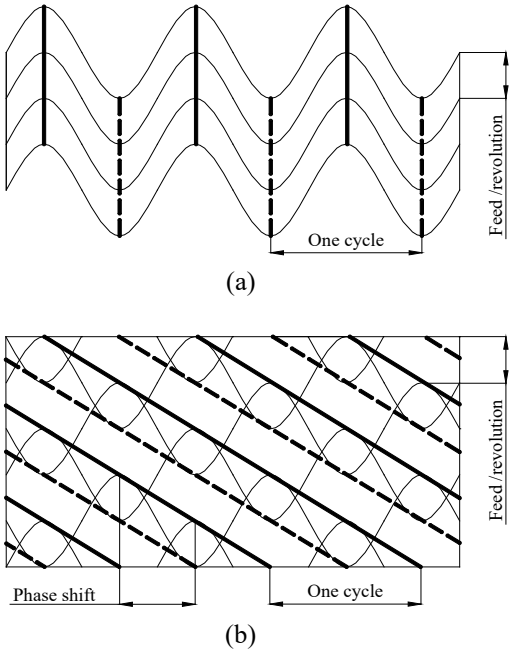

Fig. 5 Wave shift on the ground surface: (a) speed ratio V_2 / V_1 = Integer in phase, (b) $V_2 / V_1 \neq$ Integer out of phase

2.2 Surface Generation Model

Fig. 6 illustrates the geometry of ultra-precision surface grinding, the wheel-workpiece interaction is that the workpiece is scratched by the high spot as the grinding wheel traverses the workpiece under relative vibration between the wheel and the workpiece. The surface topography of the ground surface is the envelope of those scratches as shown in Fig. 1. For the theoretical modeling of the kinematic trace of the high spot, two reference frames are employed with one for the high spot (X_{p1}, Y_{p1}, Z_{p1}) on the wheel while the other for workpiece (X_1, Y_1, Z_1). The cutting trajectory can be derived from the grinding geometry. Any arbitrary point p_i on the wheel can be expressed by Eq. (4) to Eq. (6) with respect to the wheel coordinate system (X_2, Y_2, Z_2).

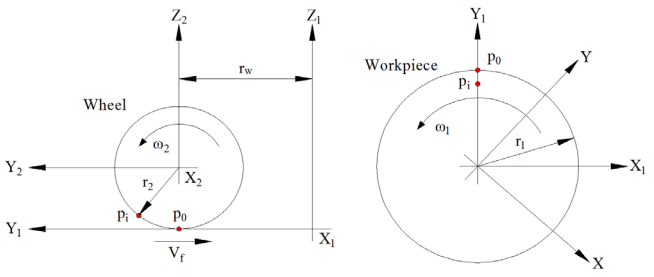

Fig. 6 The Wheel-workpiece coordinate system

$$X_2 = 0 \tag{4}$$

$$Y_2 = r_1 - r_2 \times \sin(\omega_2 t) - V_f \times t \tag{5}$$

$$Z_2 = r_2 - r_2 \times \cos(\omega_2 t) \tag{6}$$

Due to the fact that the generation of the ground surface results from the relative motion between the workpiece and the grinding wheel, the coordinate rotating transition is applied in order to use the same coordinate system. The wheel and the workpiece coordinates can be transformed to a new system (X, Y, Z), the point p_i refers to spatial position which can be derived by Eq. (7) and Eq. (8).

$$\begin{bmatrix} X \\ Y \end{bmatrix} = \begin{bmatrix} \cos(\omega_1 t) & -\sin(\omega_1 t) \\ \sin(\omega_1 t) & \cos(\omega_1 t) \end{bmatrix} \times \begin{bmatrix} X_{p1} \\ Y_{p1} \end{bmatrix} = \begin{bmatrix} \sin(\omega_1 t) \times \left(r_2 \times \sin(\omega_1 t) + V_f \times t - r_1 \right) \\ \cos(\omega_1 t) \times \left(r_1 - r_2 \times \sin(\omega_2 t) + V_f \times t \right) \end{bmatrix} \tag{7}$$

$$Z = Z_{p1} = r_2 - r_2 \times \cos(\omega_2 t) \tag{8}$$

In order to simplify the simulation work, it is supposed that only one high spot participates in the cutting of the workpiece surface in one cycle of the grinding wheel. The time interval (t_w) of the wheel acting on the surface is obtained by Eq. (9), an angle Φ that the part rotates within the time (t_w) can be expressed in Eq. (10).

$$t_w = \frac{60}{V_2} \tag{9}$$

$$\Phi = \frac{2\pi V_1}{V_2} \tag{10}$$

2.3 Surface measurement setups

Nexview 3D laser interferometric surface profiler produced by Zygo Corporation (in USA) excels at measuring both of rough and super-smooth surfaces with sub-nanometer accuracy, which is used to measure the surface topography after grinding tests. The arithmetical mean deviation for a surface (Sa) and a line roughness profile (Ra) is used to assess the machined surface quality and verify the theoretical model.

3 Experimental Design and Setup

To verify the theoretical model of surface generation in ultra-precision grinding, a series of grinding experiments were conducted on a Moore Nanotech 450UPL ultra-precision grinding machine. This machine can be used to perform ultra-precision micro-grinding of optical materials as shown in Fig. 7 A grinding wheel moves in one direction (Z axis) with a rotary axis (B axis). Workpiece is held by a vacuum chuck which moves along X axis (cross feed). The wheel diameter and thickness is 20 mm and 5 mm respectively, with an arc (nose radius 0.5 mm) in the cutting edge. The grinding conditions and mechanical properties of SiC are summarized in Table 1 and Table 2, respectively.

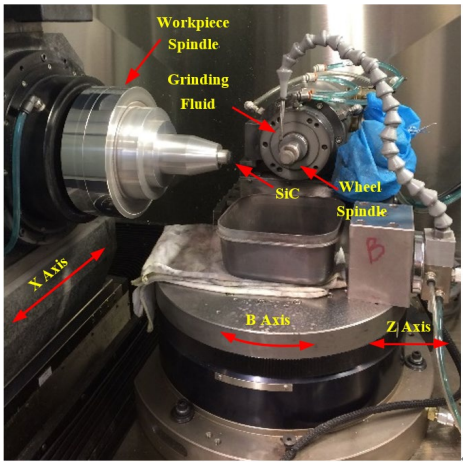

Fig. 7 Configuration of ultra-precision grinding machine

Table 1 Grinding conditions

Grinding Wheel	Resin bonded diamond wheel: #500 , diameter: 20mm, thickness: 5mm, nose radius: 0.5 mm
Rotational speed of the grinding wheel (V_2) (RPM)	40000
Rotational speed of the workpiece (V_1)(RPM)	500,1000,1500
Feed rate (V_f) (mm per min)	5,10,15
Depth of cut (H) (μm)	10
Nose radius (μm)	500

Table 2 Material properties of SiC

Workpiece	Pressureless sintering SiC
Young's modulus (H) (GPa)	430
Vickers hardness (H_v) (GPa)	28
Fracture toughness (K_{IC})(MPa·m^{½})	0.603
Density(g/cm^3)	3.2
Dimension	13 mm× 9 mm× 5mm

3 Results and Discussion

3.1 Simulation results

An eddy current probe is used to measure the fluctuation of the wheel shank by placing it near to the grinding wheel. It is found that the vibration amplitude is about 2μm under all experiments. Fig. 8 shows the simulation results of the surface patterns under different grinding conditions. For the integer number N, the surface waviness generated on the workpiece appears in the same angular position for every revolution of the workpiece. There is no phase shift as shown in Fig. 8 (a) and Fig. 8(b). If N is a non-integer, there is a small increment in the workpiece periphery with respect to the previous revolution of the workpiece, the phase shift occurs as shown in Fig. 8 (c).

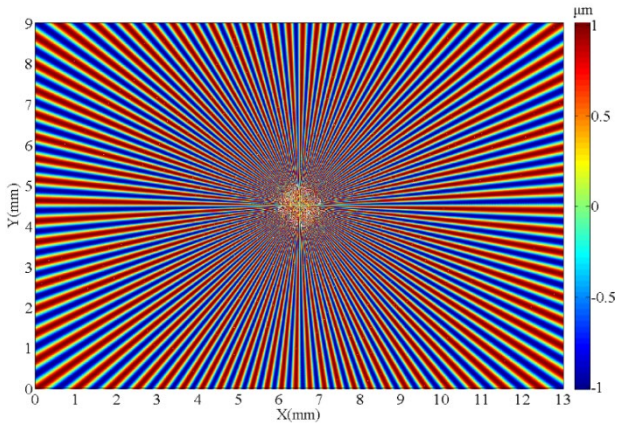

(a)

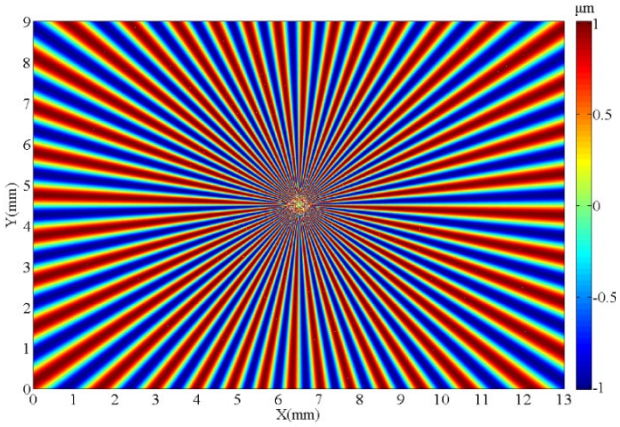

(b)

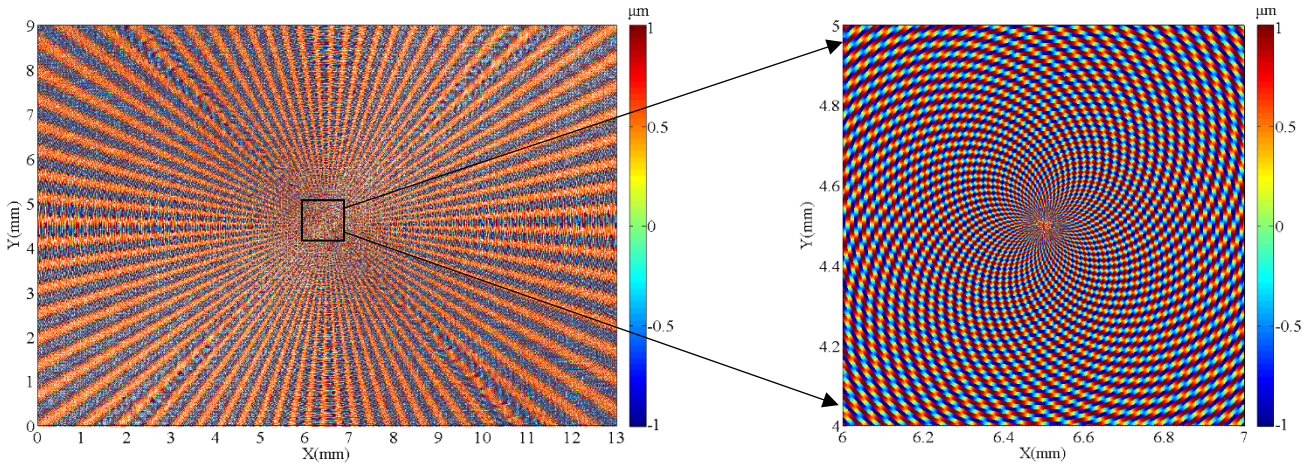

(c)

Fig. 8 Simulated surface patterns under rotational speed of the grinding wheel: 40000 RPM, feed rate: 15mm/ min, depth of cut: 10μm, rotational speed of the workpiece of (a) 500 RPM, (b) 1000 RPM, (c) 1500 RPM.

However, in the actual grinding operation, the coincidence of the integral ratio of the rotational speed of the grinding wheel to that of the workpiece is impossible due to the error motions of the spindles. The grinding tool causes relatively greater errors than the workpiece spindle. In the experiment, an average rotational speed of the grinding

wheel is used through a recording of 10 error values. It is found that the rotational speed error is about 40 RPM larger than the nominal value. This infers that a phase shift inevitably involves in the evolution of surface generation. Considering the rotational speed error of the grinding wheel, the time interval is revised in the simulation. It is interesting to note that the simulation results agrees well with the experiment results as shown in Fig. 9 to Fig. 11.

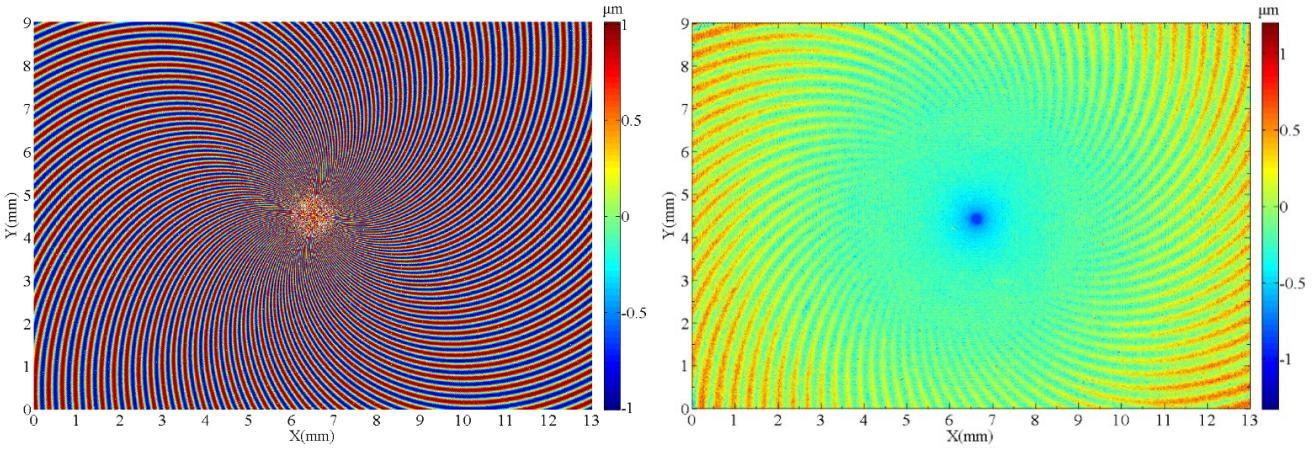

(a) (b)

Fig. 9 Contour maps for (a) the simulated surface pattern considering the rotational speed error of the grinding wheel (rotational speed of the grinding wheel: 40040 RPM) and (b) measured surface pattern (Feed rate: 15mm per min, rotation speed of the workpiece: 500 RPM, depth of cut: 10μm)

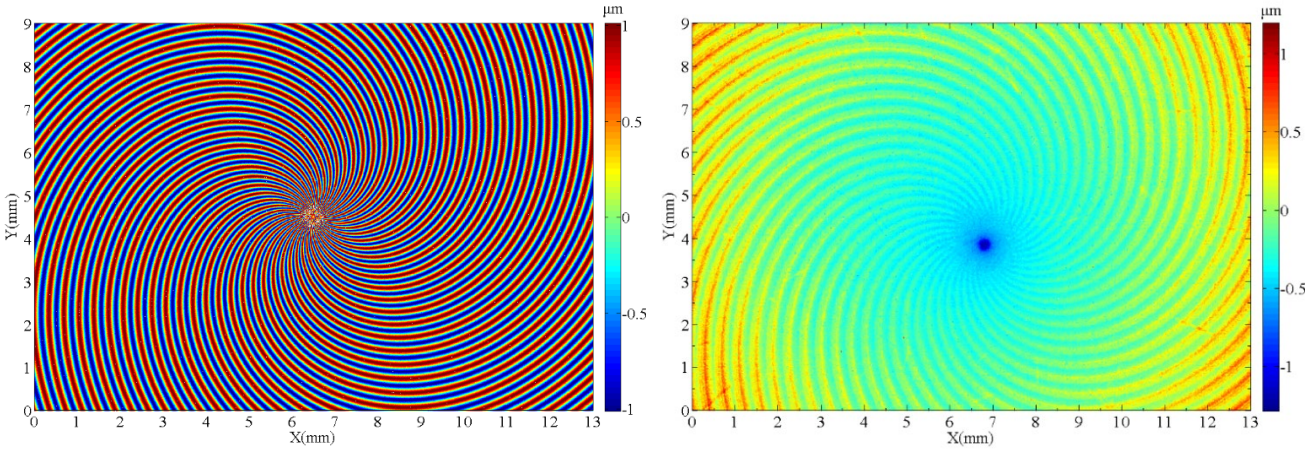

(a) (b)

Fig. 10 Contour maps for (a) the simulated surface pattern considering the rotational speed error of the grinding wheel (rotational speed of the grinding wheel: 40040 RPM) and (b) measured surface pattern (Feed rate: 15mm per min, rotational speed of the workpiece:1000 RPM, depth of cut: 10μm)

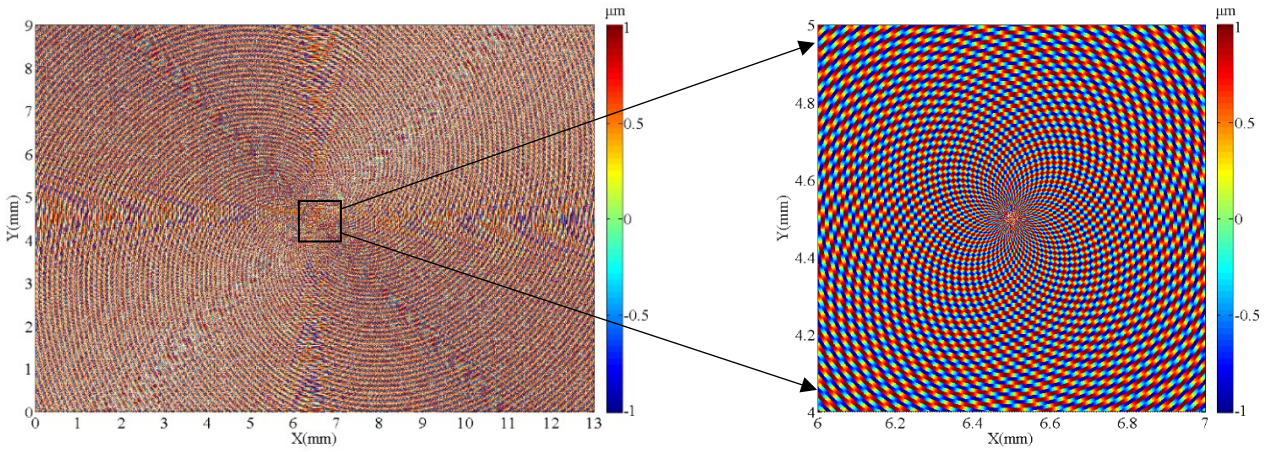

(a)

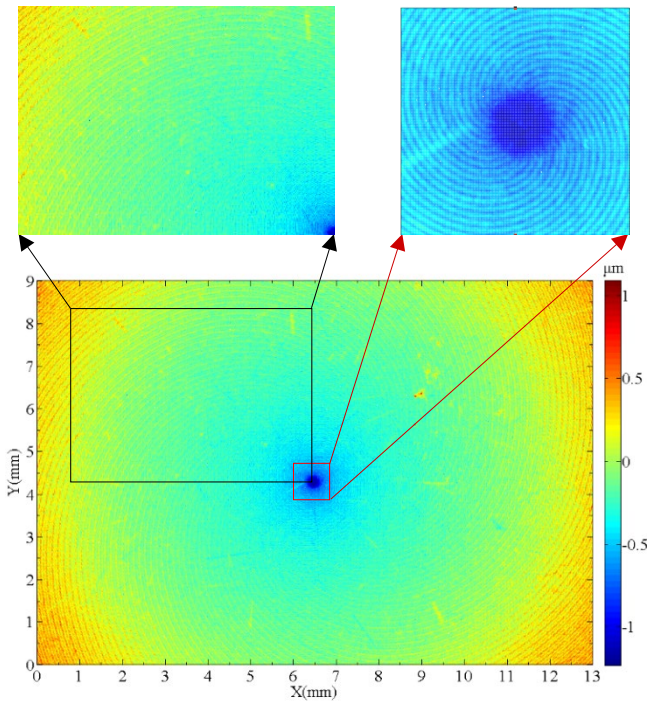

(b)

Fig. 11 Contour maps for the simulated surface pattern (a) considering the rotational speed error of the grinding wheel (rotation speed of the grinding wheel: 40040 RPM) and (b) measured surface pattern (Feed rate: 15mm/ min, rotational speed of the workpiece: 1500 RPM, depth of cut: 10μm)

Arithmetical mean height of the surface (Sa) is predicted, for an integer speed ratio, it's value is significantly larger than that of non-integer ratio, as shown in Fig. 12. Meanwhile, the simulated surface profiles (vertical to the machining direction) show that smaller phase shift (rotational speed error of the grinding wheel) in Fig. 13 (a) and Fig. 13(c) can result in a larger waviness structure of the ground surface. However, the larger phase shift as shown in Fig. 13 (e) can contribute to a dense waviness of the machined surface, which agrees well with the measured results. The deviation of the surface amplitudes may results from deformation or wear of the grinding wheel in the cutting zone. The surface profile is generated with a lower amplitude as shown in Fig. 13(f). It infers that the phase shift is beneficial

to suppress the profile fluctuation. According to the grinding theory, the surface roughness deteriorates with an increase of the relative speed between the grinding tool and the workpiece [26]. However, the surface profiles in Fig. 14 (c) shows a significant improvement in 1500RPM for the workpiece spindle, which indicates that the phase shift is also beneficial to achieve better surface finish.

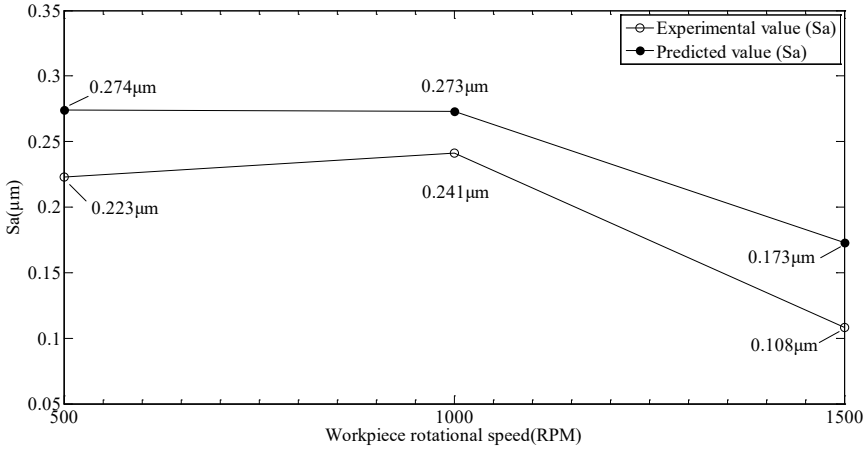

Fig. 12 A comparison between the predicted and measured arithmetical mean height of the surface (Sa) under different workpiece speeds

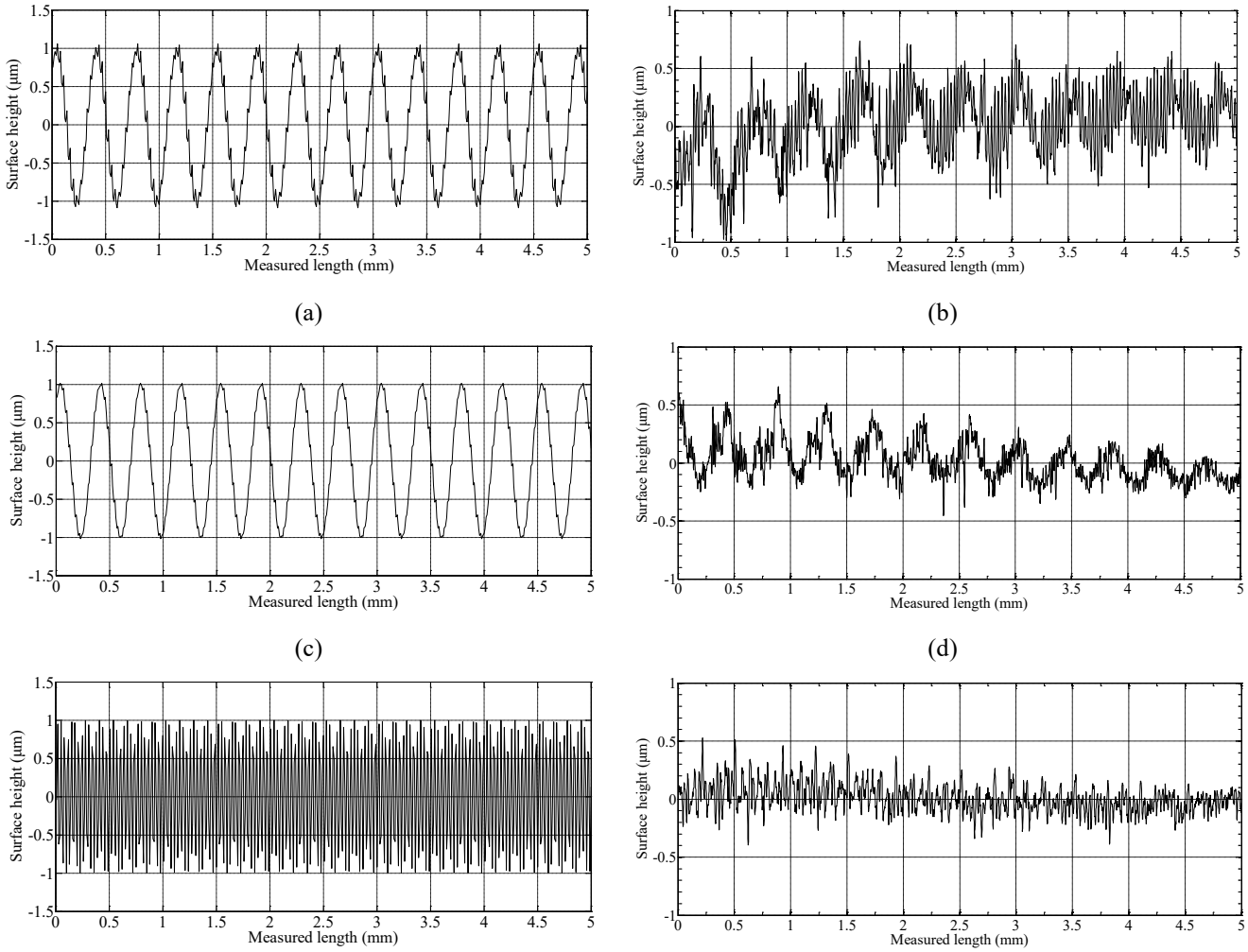

(e) (f)

Fig. 13 Surface amplitude profiles (vertical to the machining direction), (a), (c), (e) simulated and (b), (d), (f) measured profile, rotational speed of the grinding wheel: 40000 RPM, feed rate: 15mm per min, depth of cut: 10μm, rotational speed of the workpiece: (a) and (b) 500 RPM, (b) and (c) 1000 RPM, (e) and (f) 1500 RPM.

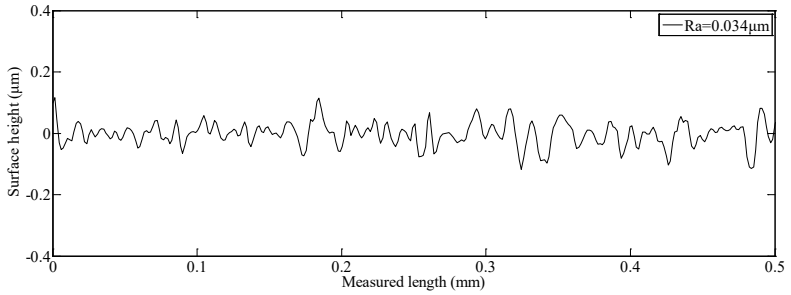

(a)

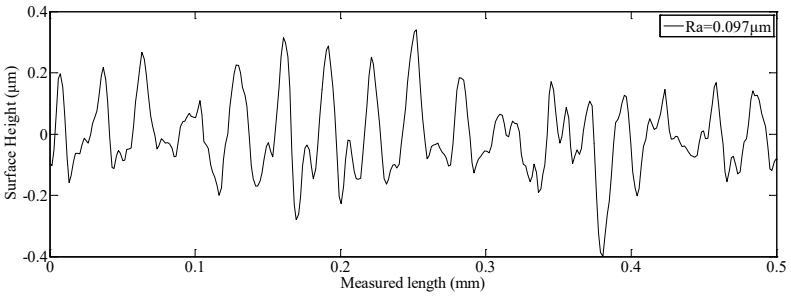

(b)

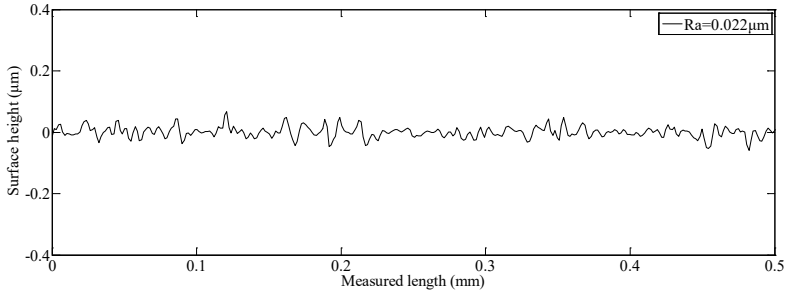

(c)

Fig. 14 Surface profiles (vertical to the machining direction) under rotational speed of the grinding wheel: 40000 RPM, feed rate: 15mm/ min, depth of cut: 10μm, rotational speed of the workpiece: (a) 500 RPM, (b) 1000 RPM, (c) 1500 RPM.

3.3 Spectral analysis of surface pattern

In order to obtain the spatial information of the ground surface in frequency domain, a series of experiments under various grinding conditions are conducted. The spectral analysis is used to uncover the periodic structures of the 3D-surface topography. A discrete fourier transform (DFT) is employed to determine the power spectrum density (PSD), which evaluates the power of a signal distributed over frequencies. A hanning window is used to evaluate the PSD so as to make the spectral intensity concentrate on its primary frequency domain.

The phase shift φ related to the ratio between the rotational speed of the grinding wheel to the rotational speed of the workpiece can be expressed in Eq. (11) [27].

$$\varphi = 2\pi|\varepsilon| \tag{11}$$

Where ε is the decimal fraction of the speed ratio in the range $-0.5 \le \varepsilon \le 0.5$, which is given as below.

$$\frac{V_2}{V_1} = N \pm \varepsilon \tag{12}$$

Where N is an integer.

The frequency of the machined surface waviness f can be expressed as

$$f = \frac{\varphi V_1}{2\pi V_f} \tag{13}$$

From Eq.s (11), (12) and (13), the frequency of surface waviness f can be re-expressed as

$$f = \frac{V_2 - N \times V_1}{V_f} \tag{14}$$

According to the Eq. (14), the frequency of the waviness of the ground surface caused by the vibration of grinding wheel is inversely proportional to the feed speed. As shown in Fig .15, as the feed rate increases (from 5mm/min to 15mm/min), the frequency of the ground surface waviness decreases from 80.91 cycles per mm to 27.01 cycles per mm, as shown in Fig. 15(a). However, the various depths of cut impose undistinguished influence on the waviness frequency as shown in Fig. 15(b). It is found in Fig. 15(c) that the frequency of the surface waviness keep stable at 9.858 cycles and 10.45 cycles per mm for the rotational speed of the workpiece at 500RPM and 1000RPM, respectively, which is consistent with the Eq. (14) and Table 3.

There are two types of frequencies for the surface waviness keep approximately constant in all ranges of machining parameters, one is the lowest frequencies (f_{11},f_{21} f_{31}) and another is the middle frequencies (f_{12},f_{22} f_{32}). The lowest frequency is related to the form accuracy (approximately equal to 0.0835 cycles per mm). It demonstrates that the slow deformation of the wheel shank traversed the workpiece contributes to the surface form error (V errors). This deformation may result from the changes of the volumetric material removal rate, which impose a proportional force for the tool shank deflection, as shown in Fig. 16. The middle frequencies (f_{12},f_{22} f_{32}) can be attributed to the micro vibration of the workpiece spindle.

Table 3 Comparison between the surface profiles in frequency domain

Machining parameters			Predicted frequency (Cycles per mm)	Measured frequency (Cycles per mm)
Feed rate (mm/min)	Depth of cut (μm)	Rotational speed of the workpiece (RPM)		

5	10	1500	92	81.03
10	10	1500	46	40.52
15	10	1500	30.67	27.01
5	5	1500	92	81.03
5	10	1500	92	81.23
5	15	1500	92	81.15
5	10	500	8.00	9.858
5	10	1000	8.00	10.45
5	10	1500	92	80.99

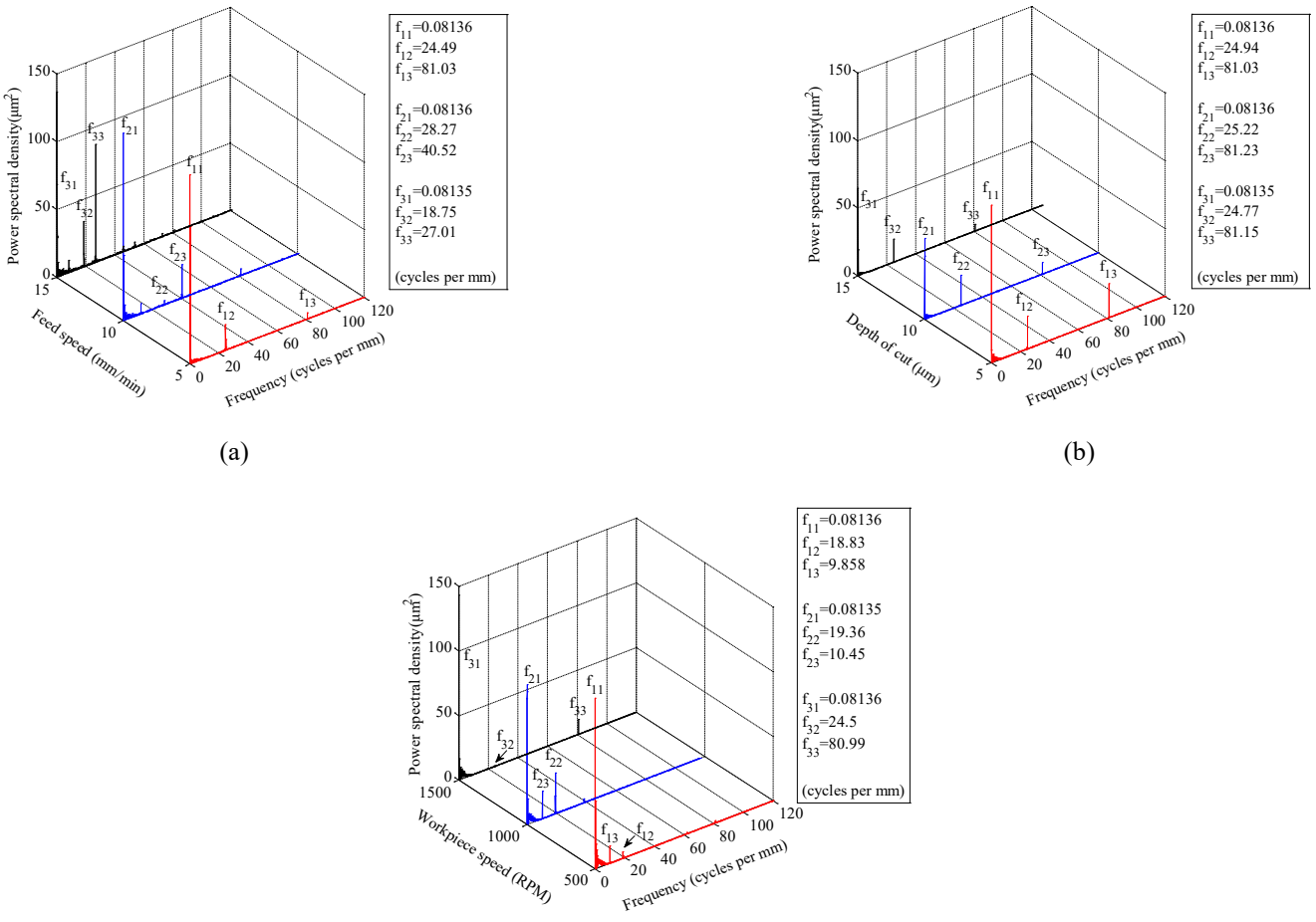

Fig. 15 Power spectral plots for the surface profile under various grinding parameters (wheel speed 40000 RPM)

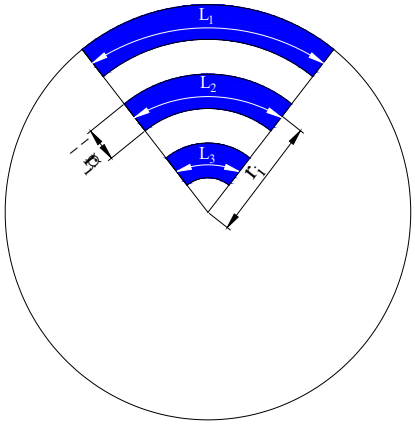

Fig. 16 Graphic representation of diverse volume material removal rates in different radial positions

In order to verify the influence of the phase shift on surface finish in grinding SiC, the rotational speed of the workpiece is set at 1500 RPM. The rotational speed of the grinding wheel is adjusted from 39000 to 40500 RPM to make the ratio of speed changes from 0.1 to 1.0 respectively. As shown in Fig. 17, it is clearly observed that a smaller change of the rotational speed of the grinding wheel can produce significant effect on the surface finish. As the phase increases from 0-0.6, the surface roughness improves. However, the surface quality degrades from 0.6-1.0. It infers that phase shift has significant influence on surface finish in ultra-precision grinding.

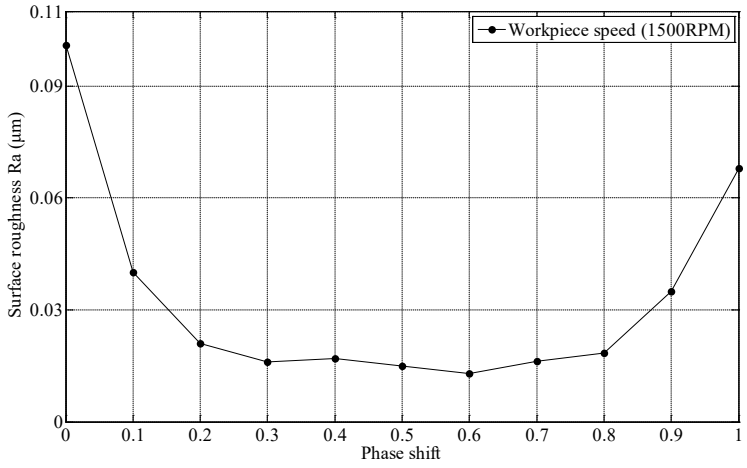

Fig .17. Influence of phase shift on surface roughness

4 Conclusions

In this paper, a comprehensive model and simulation of surface generation in ultra-precision grinding of SiC has been undertaken by taking into account of the tool geometry, tool micro-vibration and phase shift in grinding operation to uncover the evolution of surface pattern generation. It is shown that the geometric shape of spiral marks is closely related to the machining parameters (feed rate, the ratio of part speed and tool velocity). The simulation results agree well with the experimental surface patterns and the results of the spectral analysis provides the further evidence for the verification of the

model.

In addition, the phase shift is inevitably induced in the surface generation due to the small variation of the rotational speed of the grinding wheel, which is responsible for the accumulation of spiral marks in grinding. The phase shift has significant effect on the surface quality, a medium phase shift .can suppress the surface fluctuation and reduce the scallop-height of ground surface so as to acquire a good surface finish. At the same time, Fig .error (V error) caused by deflection of the tool shank due to linear variation of volume material removed rate contributes to the evolution of form error of the ground surfaces.

Acknowledgments

The work was supported by a PhD studentship (project account code: RU3K) and an MPhil studentship (project account code: RU7J) from The Hong Kong Polytechnic University. This research work was also supported by the State Key Basic Research and Development Program, China (973 program, Grant no. 2011CB 013202) and Guangdong Provincial Department of Science and Technology, Guangdong, P.R. China for The Introduction of Innovative R&D Team Program of Guangdong Province (Project no.:201001G0104781202).

References

[1] Beaucamp A, Namba Y, Combrinck H, Charlton P, Freeman R (2014) Shape adaptive grinding of CVD silicon carbide. Annals of CIRP 63:317–320

[2] Agarwal S, Rao PV (2008) Experimental investigation of surface/sub-surface damage formation and material removal mechanisms in SiC grinding. International Journal of Machine Tools & Manufacture 48:698–710

[3] Kasuga H, Ohmori H, Mishimal T, Watanabe Y, Lin W (2009) Investigation on mirror surface grinding characteristics of SiC materials. Ceramic Processing Research 10 (3):351-354

[4] Dierickx P (2000) Optical fabrication in the large. Proceedings of the SPIE 5382:224–236

[5] Saxena KK, Agarwal S, Khareb SK (2016) Surface characterization, material removal mechanism and material migration study of micro EDM process on conductive SiC. Procedia CIRP 42:179 – 184

[6] Cao JG, Wu YB, Lu D, Fujimoto M, Nomura M (2014) Fundamental machining characteristics of ultrasonic assisted internal grinding of SiC ceramics. Materials and Manufacturing Processes 29:557–563

[7] Yan JW, Zhang ZY, Kuriyagawa T (2009) Mechanism for material removal in diamond turning of reaction-bonded silicon carbide. International Journal of Machine Tools & Manufacture 49:366–374

[8] Tam HY, Cheng HB, Wang YW (2007) Removal rate and surface roughness in the lapping and polishing of RB-SiC optical components. Journal of Materials Processing Technology 192–193:276–280

[9] Dai Y, Ohmori H, Lin W, Eto H, Ebizuka N, Tsuno K (2005) ELID grinding properties of high-strength reaction-sintered SiC. Key Engineering Materials 291–292:121–126

[10] Pan GS, Zhou Y, Luo GH, Shi XL, Zou CL, Gong H (2013) Chemical mechanical polishing (CMP) of on-axis Si-face 6H-SiC wafer for obtaining

atomically flat defect-free surface. International Journal of Advanced Manufacturing Technology 24:5040–5047

[11] Malkin S, Guo CS (2008) Grinding Technology: Theory and Applications of Machining with Abrasives. Industrial Press, New York

[12] Salisbury EJ, Domala KV, Moon KS, Miller MH, Sutherland JW (2001) A Three-dimensional for the Surface Texture in Surface Grinding, Part II: Grinding Wheel Surface Texture Model. Manufacture Science Engineer 123(4):582–590

[13] Wang Y, Moon KS (1997) A Methodology for The Multiresolution Simulation of Grinding Wheel Surface. Wear 211(2) :218–225

[14] Xie J, Li Q, Sun JX, Li YH (2015) Study on ductile-mode mirror grinding of SiC ceramic freeformsurface using an elliptical torus-shaped diamond wheel. Journal of Materials Processing Technology 222:422–433

[15] Subramanian K, Ramanath S, Tricard M (1997) Mechanisms of material removal in the precision production grinding of ceramics. Journal of Manufacturing Science and Engineering 119:509-519

[16] Chena JB, Fanga QH, Wanga CC, Dub JK, Liuca F (2016) Theoretical study on brittle–ductile transition behavior in elliptical ultrasonic assisted grinding of hard brittle materials. Precision Engineering (In Press)

[17] Muhammad A, Mustafizur R, Wong YS (2011) Analytical modeling of ductile-regime machining of tungsten carbide by endmilling. International Journal of Advanced Manufacturing Technology 55:53-64

[18] Blackley WS, Scattergood RO (1991) Ductile-regime machining model for diamond turning of brittle materials. Precision Engineering 13:95–103

[19] Kitahara H, Noda Y, Yoshida F, Nakashima H, Shinohara N, Abe H (2001) Mechanical behavior of single crystalline and polycrystalline silicon carbides evaluated by Vickers indentation. Journal of the Ceramic Society of Japan 109:602–606

[20] Patten J, Gao W, Yasuto K (2005) Ductile regime nanomachining of single-crystal silicon carbide. ASME Journal of Manufacturing Science and Engineering 127:522–532

[21] Bifano TG, Dow TA, Scattergood RO (1991) Ductile-regime grinding: a new technology for machining brittle materials. Journal of Engineering for Industry 113:184-189

[22] Fawcett S, Dow TA (1991) Development of a model for precision contour grinding of brittle materials. Precision Engineering 13(4):270-276

[23] Cheng J, Gong YD (2014) Experimental Study of Surface Generation and Force Modeling in Micro-grinding of Single Crystal Silicon Considering Crystallographic Effects. International Journal of Machine Tools and Manufacture 77:1–15

[24] Jiang J, Ge P, Hong J (2013) Study on Micro-interacting Mechanism Modeling in Grinding Process and Ground Surface Roughness Prediction. International Journal of Advanced Manufacturing Technology 67(5):1035–1052

[25] Chen JB, Fang QH, Li P (2015) Effect of Grinding Wheel Spindle Vibration on Surface Roughness and Subsurface Damage in Brittle Material Grinding. International Journal of Machine Tools and Manufacture 91:12-23

[26] Malkin S (2008) Grinding Technology: Theory and Applications of Machining with Abrasives. Industrial Press, 2nd edn

[27] Cheung CF, Lee WB (2000) A Theoretical and Experimental Investigation of Surface Roughness Formation in Ultra-precision Diamond Turning. International Journal of Machine Tools and Manufacture 40(7):979–1002